Potential relationship between high wall shear stress and plaque rupture causing acute coronary syndrome

Yusuke Fukuyama
Kobe University Graduate School of Medicine School of Medicine: Kobe Daigaku Daigakuin Igakukei Kenkyuka Igakubu

Hiromasa Otake (hotake@med.kobe-u.ac.jp)
Kobe University Graduate School of Medicine

Fumiyasu Seike
Ehime University Graduate School of Medicine School of Medicine: Ehime Daigaku Daigakuin Igakukei Kenkyuka Igakubu

Hiroyuki Kawamori
Kobe University Graduate School of Medicine School of Medicine: Kobe Daigaku Daigakuin Igakukei Kenkyuka Igakubu

Takayoshi Toba
Kobe University Graduate School of Medicine School of Medicine: Kobe Daigaku Daigakuin Igakukei Kenkyuka Igakubu

Yu Takahashi
Kobe University Graduate School of Medicine School of Medicine: Kobe Daigaku Daigakuin Igakukei Kenkyuka Igakubu

Kyohei Sasabe
Ehime University Faculty of Engineering Graduate School of Science and Engineering: Ehime Daigaku Kogakubu Daigakuin Rikogaku Kenkyuka

Keisuke Kimura
Ehime University Faculty of Engineering Graduate School of Science and Engineering: Ehime Daigaku Kogakubu Daigakuin Rikogaku Kenkyuka

Junya Shite
Saiseikai Nakatsu Hospital: Saiseikai Nakatsu Byoin

Amane Kozuki
Saiseikai Nakatsu Hospital: Saiseikai Nakatsu Byoin

Masamichi Iwasaki
Hyogo Prefectural Awaji Hospital: Hyogo Kenritsu Awaji Iryo Center

Tomofumi Takaya
Hyogo Brain and Heart Center: Hyogo Kenritsu Himeji Junkankibyo Center

Kazunori Yasuda
Ehime University Faculty of Engineering Graduate School of Science and Engineering: Ehime Daigaku Kogakubu Daigakuin Rikogaku Kenkyuka
Osamu Yamaguchi
Ehime University Graduate School of Medicine School of Medicine: Ehime Daigaku Daigakuin Igakukei Kenkyuka Igakubu
Ken-ichi Hirata
Kobe University Graduate School of Medicine School of Medicine: Kobe Daigaku Daigakuin Igakukei Kenkyuka Igakubu

---

Research Article

Keywords: Acute coronary syndrome, Plaque rupture, Optical coherence tomography, Computational fluid dynamics, Wall shear stress

Posted Date: June 18th, 2021

DOI: https://doi.org/10.21203/rs.3.rs-629630/v1

Abstract

Purpose: To investigate the detailed relationship between high wall shear stress (WSS) and plaque rupture (PR) in longitudinal and circumferential locations.

Methods: Overall, 100 acute coronary syndrome (ACS) patients whose culprit lesions had PR documented by optical coherence tomography (OCT) were enrolled. Lesion-specific three-dimensional coronary artery models were created using OCT data. At the ruptured portion, tracing of the luminal edge of the residual fibrous cap was smoothly extrapolated to reconstruct the luminal contour before PR. Then, WSS was computed from computational fluid dynamics analysis. PR was classified into central-PR and lateral-PR according to the disrupted fibrous cap location.

Results: In the longitudinal 3-mm segmental analysis, multivariate analysis demonstrated that higher WSS in the upstream segment was independently associated with Upstream-PR and a thinner fibrous cap was independently associated with Downstream-PR. In PR cross-sections, PR region had a significantly higher average WSS than the non-PR region. In the cross-sectional analysis, peak WSS was most frequently observed in the *lateral* region (66.7%) in lateral-PR, whereas that in central-PR was most frequently observed in the *central* region (70%). Multivariate analysis demonstrated that the presence of peak WSS at the *lateral* region, thinner broken fibrous cap, and larger lumen area were independently associated with lateral-PR, while the presence of peak WSS at the *central* region and thicker broken fibrous cap were independently associated with central-PR.

Conclusions: A combined approach with computational fluid dynamics simulation and morphological plaque evaluation by OCT might help predict future PR-induced ACS events.

Introduction

Coronary plaque rupture (PR) is the most common mechanism leading to acute coronary syndrome (ACS) [1]. Several morphological characteristics, including a thin fibrous cap, large necrotic core, and foamy macrophage infiltration, are considered potential features of rupture-prone vulnerable plaques [2]. Recent studies have demonstrated that high wall shear stress (WSS) is associated with plaque vulnerability progression and PR onset [3-5]. However, these studies speculate the potential relationship between high WSS and atherosclerotic progression by averaging the WSS in longitudinal and circumferential directions in vessel segments, while WSS often varies significantly in longitudinal and circumferential directions within a luminal narrowing region. The direct relationship between regional WSS and local plaque findings, including the location of fibrous cap disruption and thin-cap fibroatheroma (TCFA), remains uncertain.

Optical coherence tomography (OCT) is an intracoronary imaging modality that can provide in vivo high-resolution coronary plaque images; it can clearly visualize the exact location of fibrous cap disruption in PR lesions and TCFA [6]. We developed a novel WSS assessment method using OCT-derived lumen profiles. This method employs computational fluid dynamics (CFD) analysis over the entire patient-

specific three-dimensional coronary model generated from two-dimensional OCT data and preserves the exact correspondence between the CFD solution and OCT data; it has a high potential to assess the relationship among PR, TCFA, and WSS more accurately and directly than conventional techniques. Therefore, we aimed to investigate the detailed relationships among PR, TCFA, and WSS in patients who underwent OCT for ACS culprit lesions with PR.

Methods

Study design and patient population

The Kobe OCT ACS registry is a multicentre, retrospective observational registry that could be used to evaluate the morphological characteristics of ACS culprit lesions in patients undergoing primary percutaneous coronary intervention for ACS (UMIN000038442). Totally, 443 patients were enrolled in the registry from four Japanese institutions (Online Resource 1). Among them, 145 consecutive ACS patients whose culprit lesions had PR documented by OCT were screened. ACS was defined as unstable angina, non-ST elevation myocardial infarction, and ST elevation myocardial infarction.

The exclusion criteria were in-stent restenosis, coronary artery bypass grafting, insufficient OCT image quality, culprit lesion predilated with a balloon prior to OCT imaging, and ruptured plaques that were insufficient to reconstruct three-dimensional models.

Lesion-specific three-dimensional coronary artery models were created using OCT data. WSS was computed with CFD analysis by a single core laboratory (Ehime University, Toon, Japan). We retrospectively collected all data from patient records.

OCT image acquisition and analysis

After thrombus aspiration, OCT imaging and off-line OCT analysis were performed as previously described [6]. OCT images were analyzed by two independent investigators (YF, YT), blinded to the clinical presentation, using validated plaque characterization criteria. PR was defined as the presence of a fibrous cap discontinuity with a clear cavity formed inside the plaque. At the ruptured portion, broken fibrous cap thickness was measured at the site where the fibrotic cap remnant was thinnest (Fig. 1). Online Resource 1 presents a detailed OCT analysis.

Three-dimensional geometry reconstruction and CFD simulations

Lesion-specific three-dimensional coronary artery models were created using cross-sectional OCT images by tracing the luminal contour. Specifically, at the ruptured portion, the tracing of the luminal edge of the residual fibrous cap was smoothly extrapolated to reconstruct the luminal contour before PR. We selected the ruptured plaques with a significant amount of residual fibrous cap to accurately reconstruct the original vessel. To avoid inaccurate reconstruction of the original vessel, plaques with irregular flaps too protruding into the lumen or excessive deformation were excluded. CFD analysis was performed using

ANSYS Fluent (ANSYS, Inc., PA, USA). Detailed three-dimensional geometry reconstruction and CFD simulations are shown in Online Resources 1 and 2.

Relationship between WSS and PR and TCFA locations

Relationships between WSS and PR and TCFA locations were assessed using the following two methods. Two independent investigators (KS, KK) performed these analyses blinded to the clinical presentation; discordance was resolved by consensus.

1) Longitudinal 3-mm segmental analysis

Each culprit lesion was subdivided into five 3-mm segments with respect to the minimum lumen area (MLA) location at the central segment. To investigate the regional impact of the luminal narrowing on the relationship between WSS and PR, we focused on the segment with MLA and two consecutive segments: proximal (upstream: UP1, UP2) and distal (downstream: DN1, DN2) segments (Fig. 2A). The average WSS was calculated for each 3-mm segment. All lesions were classified into Upstream-PR, MLA-PR, and Downstream-PR according to the PR's longitudinal location (Online Resource 1); the 3-mm segments where the PR was located were subdivided into cross-sections with and without PR, and the average WSS was compared between them (Fig. 2A).

2) Circumferential analysis of the relationship among WSS, PR, and TCFA

On each PR cross-section, the vessel wall was divided into two circumferential regions: PR and non-PR. In the PR region, the ruptured plaque cavity could be clearly detected (Fig. 2B, C). We measured the maximum, average, and minimum WSS values in each region (PR and non-PR regions) on every PR cross-section (Fig. 2C).

We also included all cross-sections with plaques that had TCFA if the plaques were located >10 mm apart from the ACS culprit plaques (Online Resource 2A-2). The average WSS of the cross-sections with and without TCFA and of the TCFA and non-TCFA regions was similarly calculated.

Relationship between the peak WSS location and PR types

In each PR lesion, the cross-sections with peak WSS, in which the highest WSS was located, were selected (Fig. 2A). On such cross-sections, the vessel wall was circumferentially divided into subregions. The PR regions were divided into three equally separate subregions: *central* and two *lateral* regions; the non-PR region was divided into two *semi-lateral* and *other* regions (Fig. 2B). The location of the peak WSS value was determined according to these regions (*central*, *lateral*, *semi-lateral*, or *other*). In the same cross-section, each PR was classified into three types according to disrupted fibrous cap location. Central-PR (C-PR) and lateral-PR (L-PR) were defined as PRs whose disrupted fibrous caps were located at the *central* and *lateral* regions, respectively. Other-PR was defined as a not classifiable PR due to the lack of a detectable fibrous cap disruption site because of imaging artifacts or massive thrombus presence (Fig. 1,

2) [7]. In cases with different PR types in different cross-sections within the same lesions, the aforementioned classification of peak WSS cross-section was employed.

Statistical analysis

Statistical analyses (Online Resource 1) were performed using SPSS for Windows version 26 (IBM SPSS Inc., Chicago, IL, USA). In the longitudinal 3-mm segmental analysis, univariate and multivariate analyses were implemented to identify the parameters associated with each longitudinal PR type. In the circumferential analysis, univariate and multivariate analyses were implemented to identify the parameters associated with L-PR or C-PR. In each statistical test other than the post-hoc analysis of categorical data, the significance level was set at $p<0.05$, and a 95% confidence interval (CI) was reported, unless otherwise stated.

Results

Baseline characteristics

Among the 145 consecutive ACS patients, 45 were excluded because of in-stent restenosis (n = 6), insufficient OCT image quality (n = 15), culprit lesions predilated with a balloon prior to OCT imaging (n = 9), and ruptured plaques that were insufficient to reconstruct the three-dimensional models (n = 15). Finally, 100 ACS patients with PR detected by OCT were enrolled; of those, 30 had TCFA in lesions > 10 mm away from the ACS culprit plaque. The baseline characteristics are summarised in Online Resource 3.

Longitudinal 3-mm Segmental Analysis

The incidences of Upstream-PR, MLA-PR, and Downstream-PR were 45%, 40%, and 15%, respectively. The highest average WSS in Upstream-PR was in UP1 and that in MLA-PR was in the MLA segment (Table 1). In Downstream-PR, the highest WSS was in the MLA segment, followed by DN1. Regarding OCT findings, the broken fibrous cap was significantly thinner and the peak WSS was significantly lower in Downstream-PR (Online Resource 4). On multivariate analysis, higher WSS at UP1 was independently associated with Upstream-PR development (odds ratio [OR] = 1.05; 95% CI = 1.01–1.09; p = 0.007), and thinner fibrous cap was independently associated with Downstream-PR development (OR = 0.95; 95% CI = 0.92–0.98; p = 0.004).

Table 1
Comparisons of the average wall shear stress among the longitudinal 3-mm segments

	Downstream-2	Downstream-1	MLA	Upstream-1	Upstream-2	p-value
Total-PR (n = 100)	5.5 (4.6–6.7)	6.9 (5.7–8.3)	18.3 (15.2–22.0)	15.8 (13.1–19.0)	5.9 (4.9–7.1)	< 0.001
Upstream-PR (n = 45)	6.0 (4.6–7.8)	7.0 (5.4–9.1)	19.0 (14.6–24.8)	20.4 (15.6–26.5)	7.0 (5.4–9.1)	< 0.001
MLA-PR (n = 40)	5.1 (3.8–6.8)	5.8 (4.3–7.7)	18.2 (13.6–24.4)	13.9 (10.4–18.7)	5.4 (4.0-7.2)	< 0.001
Downstream-PR (n = 15)	5.3 (3.2–8.7)	10.4 (6.3–17.2)	16.1 (9.6–26.7)	8.3 (5.0-13.7)	4.7 (2.8–7.7)	< 0.001
TCFA (n = 30)	1.6 (1.2–2.3)	1.9 (1.3–2.7)	3.2 (2.3–4.6)	2.8 (2.0-4.1)	1.9 (1.3–2.7)	< 0.001

Values expressed as average (95% confidence interval).

MLA, minimum lumen area; PR, plaque rupture; TCFA, thin-cap fibroatheroma

Circumferential analysis of the relationship among WSS, PR, and TCFA

A total of 1470 PR cross-sections and 1830 non-PR cross-sections were analyzed. The average WSS of the PR cross-section was significantly higher than that of the non-PR cross-sections (18.9 [16.1–22.4] Pa vs. 8.8 [7.3–10.4] Pa, $p < 0.001$; Fig. 3A). In the PR cross-sections, the average WSS of the PR region was significantly higher than that of the non-PR region (21.3 [17.7–25.6] Pa vs. 16.8 [14.0-20.3] Pa, $p < 0.001$; Fig. 3B). Additionally, 385 TCFA cross-sections and 590 non-TCFA cross-sections were analyzed. The average WSS of the TCFA cross-section was significantly higher than that of the non-TCFA cross-sections (2.8 [1.9–4.1] Pa vs. 2.3 [1.6–3.3] Pa, $p < 0.001$; Fig. 3A) but significantly lower than that of the PR cross-sections. In the TCFA cross-sections, the average WSS of the TCFA region was significantly higher than that of the non-TCFA region but significantly lower than that of the PR regions (3.1 [2.2–4.4] Pa vs. 2.4 [1.7–3.4] Pa, $p < 0.001$, Fig. 3B). Detailed WSS measurements in the PR and TCFA cross-sections are summarised in Online Resource 5.

Circumferential analysis of the relationship between WSS and PR types

Among the 100 lesions with PR, 51 (51%) were classified as L-PR, 42 (42%) as C-PR, and 7 (7%) as other-PR. The peak WSS was most frequently observed in the *lateral* region (66.7%), followed by the *semi-lateral* region (13.7%) in L-PR and in the *central* region (70%) in C-PR (Fig. 4).

Table 2 compares the OCT and WSS-related parameters between L-PR and C-PR. Compared with C-PR, L-PR had a significantly larger lumen area at the peak WSS cross-section (1.5 [1.3-2.0] mm^2 vs. 1.4 [1.1–1.6] mm^2, p = 0.008). L-PR had a significantly thinner broken fibrous cap than C-PR (40 [30–50] μm vs. 80 [67.5–100] μm, p < 0.001). L-PR had a significantly lower peak and average WSS value than C-PR (peak WSS 44.6 [19.6–65.2] Pa vs. 84.7 [36.6-177.5] Pa, p < 0.001; average WSS 14.3 [11.2–18.3] Pa vs. 26.7 [20.4–35.1] Pa, p < 0.001) (Table 2).

Table 2
Comparisons between lateral-PR and central-PR

Characteristics	Lateral-PR	Central-PR	p-value
Reference lumen area, mm^2	5.6 (3.9–6.7)	6.5 (4.7–8.3)	0.064
Minimum lumen area, mm^2	1.25 (0.82–1.52)	1.21 (0.68–1.46)	0.975
Lumen area at peak WSS cross-section, mm^2	1.5 (1.3-2.0)	1.4 (1.1–1.6)	0.008
Broken fibrous cap thickness, μm	40 (30–50)	80 (67.5–100)	< 0.001
Average WSS of PR cross-section [a], Pa	14.3 (11.2–18.3)	26.7 (20.4–35.1)	0.001
WSS at PR region [a], Pa	15.4 (12.1–19.7)	28.2 (21.5–37.1)	0.001
WSS at non-PR region [a], Pa	12.2 (9.5–19.7)	22.2 (16.8–29.5)	0.002
Peak WSS, Pa	44.6 (19.6–65.2)	84.7 (36.6-177.5)	< 0.001

Values are median (interquartile range) for crude analysis or average (95% confidence interval) for multilevel analysis.

[a] Assessed by multilevel analysis.

PR, plaque rupture; WSS, wall shear stress

Multivariate analysis demonstrated that the presence of peak WSS at the *lateral* region, thinner broken fibrous cap, and larger lumen area at the peak WSS cross-sections were independent parameters associated with L-PR. Moreover, the presence of peak WSS at the *central* region and thicker broken fibrous cap were independent parameters associated with C-PR (Table 3).

Table 3
Multivariate logistic regression analysis for lateral-PR and central-PR

Lateral-PR					
Characteristics	*B* (S.E.)	Wald	Odds ratios	95% CI	p-value
Presence of peak WSS at the *lateral* region [a]	2.61 (0.6)	19.54	13.64	4.28–43.45	< 0.001
Broken fibrous cap thickness	-0.03 (0.01)	9.74	0.97	0.95–0.99	0.002
Lumen area at peak WSS	1.91 (0.58)	10.83	6.74	2.16–21.03	0.001
Central-PR					
Characteristics	*B* (S.E.)	Wald	Odds ratios	95% CI	p-value
Presence of peak WSS at the *central* region [b]	3.46 (0.81)	18.34	31.84	6.53–155.2	< 0.001
Broken fibrous cap thickness	0.1 (0.02)	21.22	1.11	1.06–1.15	< 0.001

[a] *Central*, *semi-lateral*, and *other* regions were coded 0, and *lateral* region was coded 1.

[b] *Lateral*, *semi-lateral*, and *other* regions were coded 0, and the *central* region was coded 1.

CI, confidence interval; PR, plaque rupture; S.E., standard error; WSS, wall shear stress

Discussion

We investigated the potential relationships between WSS values and the location of PR or TCFA in ACS patients; by conducting CFD analysis on a three-dimensional coronary model augmented with OCT geometry, we evaluated WSS values at the exact measurement location as local OCT features were measured. Besides the traditional longitudinal 3-mm segmental comparison, we conducted a circumferential regional analysis to compare WSS values between regions with specific OCT findings and those without specific findings within the same longitudinal location. Thus, we identified a direct relationship among PR, TCFA, and local WSS distribution in ACS patients, from a global lesion level to a local level.

High WSS Is Associated With Plaque Destabilization And Rupture

In non-diseased arteries, high WSS is considered atheroprotective [8], whereas in diseased arteries with luminal narrowing, higher WSS can promote further vulnerable changes leading to TCFA [9, 10], which

could result in PR. We enrolled ACS patients with PR and demonstrated that higher WSS was associated with TCFA and PR. In several studies, high WSS can induce thinning of fibrous caps by promoting plasmin-induced metalloproteinase activity, smooth muscle cell apoptosis, decreased matrix synthesis, accelerated angiogenesis, and transformation to a vulnerable phenotype [11, 12].

Studies have demonstrated the potential contribution of high WSS to plaque vulnerability using various imaging modalities [9, 10]. However, data on the relationship between high WSS and PR is limited. A CFD study with intravascular ultrasonography of ruptured plaques in 20 ACS patients demonstrated a strong correlation between focal elevation in WSS and PR location (k = 0.79) [5]. Moreover, Kumar *et al*. [4] demonstrated that higher WSS in the proximal segments of atherosclerotic lesions is predictive of subsequent myocardial infarction occurrence within 3 years. These results indicate that high WSS may play a pivotal role in PR initiation in patients with high-risk vulnerable plaque.

In the longitudinal segmental analysis, we demonstrated that the average WSS of the PR cross-sections was significantly higher than that of the non-PR cross-sections within the same longitudinal segment. Notably, the average WSS of the PR cross-sections was significantly higher than that of the TCFA cross-sections. Although high WSS is associated with both plaque destabilization and PR, these data suggest that much higher WSS will be required to trigger the PR process.

We demonstrated that the location of the highest average WSS corresponded to the PR location in the Upstream-PR and MLA-PR. In line with our results, Kumar *et al*. [4] demonstrated that higher WSS in the proximal segments of atherosclerotic lesions is predictive of subsequent myocardial infarction occurrence. Considering that higher proximal WSS was observed in patients with subsequent myocardial infarction regardless of lesion location and morphology, it might play an important role in plaque destabilization and rupture, leading to subsequent myocardial infarction.

On the other hand, here, 15% of PR cases were observed in the downstream segment. Interestingly, in the Downstream-PR, the location of the highest WSS did not correspond to the PR location, but rather that of the second-highest WSS. These results indicate that PR may be determined by balancing several factors. In Downstream-PR, the broken fibrous cap was significantly thinner and peak WSS was significantly lower than other PR types. Therefore, we speculate that Downstream-PR could be induced with relatively lower WSS if there is a highly vulnerable plaque in the downstream segment. Generally, lower WSS is observed in the downstream segment rather than in the MLA and upstream segments; Downstream-PR might occur only if a plaque with a higher vulnerability can be broken with relatively low WSS. Further studies with larger populations are warranted for confirmation.

Direct Relationship Among WSS, Plaque Vulnerability, And PR

Hemodynamic parameters are significantly affected by several geometrical characteristics, including luminal narrowing, lesion location, and lesion length[9]. Although previous studies demonstrated a potential relationship among high WSS, plaque instability, and PR, they employed longitudinal and circumferential averaging of WSS values in a certain range. To our knowledge, no studies have clarified

the direct relationship between WSS and vulnerable plaque features by eliminating the potential influence of geometrical conditions. By comparing WSS between regions with and without specific OCT findings within the same longitudinal ranges, we could investigate the relationship more specifically and directly by eliminating the influence of geometrical factors on WSS. Accordingly, we found that WSS was significantly higher in regions with TCFA and PR than in those without the features for the same longitudinal regions with the same degree of stenosis. These data suggest the importance of high WSS on plaque destabilization and rupture regardless of geometrical factors, including lesion location and luminal narrowing.

A necropsy study[7] reported that the circumferential PR incidences at the lateral, central, and other regions were 59%, 35%, and 6%, respectively, corresponding with our results (L-PR, 51%; C-PR, 42%; other-PR 7%). Interestingly, we demonstrated co-localization of peak WSS and the site of fibrous cap disruption, which led to ACS events. In L-PR, the peak WSS was observed in the *lateral* or *semi-lateral* region in > 80% of the ruptured plaques; in C-PR, it was most frequently observed in the *central* region (70%) (Fig. 4). Although spatial co-localization is not mechanistic evidence of causality, these results suggest that identifying focal areas of high WSS over atheroma harboring other advanced morphologic features may improve the detection of plaques before symptomatic rupture.

Potential factors associated with the prediction of circumferential PR type

In the multivariate analysis, the presence of peak WSS at the *lateral* region, thinner broken fibrous cap, and larger lumen area at the peak WSS site were independently associated with L-PR. These data suggest that L-PR was induced by relatively lower WSS at a highly vulnerable plaque with a thinner fibrous cap, whereas C-PR was induced by higher WSS at a plaque with a thicker fibrous cap. In a previous autopsy study enrolling sudden death cases, Burke *et al*. [13] demonstrated that, among 16 PRs occurring on exertion, 75% (12 PRs) were C-PR, whereas, among 20 PRs occurring without exertion (rest PRs), 65% (13 PRs) occurred in the shoulder region, suggesting that physical exertion tends to shift the PR site from the shoulder to the midcap where WSS is expected to be highest. Although no direct assessment was performed on local WSS in this study, these data might support our findings that C-PR had a significantly higher peak and average WSS than L-PR. Interestingly, C-PR had a significantly smaller lumen area at the cross-section with peak WSS and a significantly thicker broken fibrous cap than L-PR. These data suggest that C-PR might occur at a plaque with a relatively thicker fibrous cap triggered with relatively high WSS, whereas L-PR can be induced by relatively low WSS because of advanced plaque vulnerability. Integrating morphological features, plaque vulnerability, and adverse hemodynamic conditions might improve the accuracy of identifying high-risk plaques that can cause future ACS.

Limitations

This study has some limitations. First, this is a retrospective, observational study with a small sample size, which might increase the possibility of selection bias. Second, WSS analysis was performed based only on OCT images without co-registration with angiography or computed tomography. Thus, the effect

of vessel tortuosity was not evaluated. However, the impact of vessel tortuosity on high WSS distribution in the severely stenotic lesion could be minimal. Nonetheless, our results could provide important mechanistic insight into the relationship between PR and WSS. Lumen tracing was performed as an implicit assumption to reconstruct the luminal contour before PR, affecting analysis results. A prospective study with serial observation is warranted to confirm our speculation.

Conclusion

OCT-based CFD simulation revealed that high WSS might be related to the longitudinal and circumferential location of PR and TCFA. Integrating morphological features, plaque vulnerability, and adverse hemodynamic conditions might improve the accuracy of identifying high-risk plaques that can cause future ACS.

Abbreviations

ACS=acute coronary syndrome

C-PR=central-plaque rupture

CFD=computational fluid dynamics

CI=confidence interval

DN=downstream

L-PR=lateral-plaque rupture

MLA=minimum lumen area

OCT=optical coherence tomography

OR=odds ratio

PR=plaque rupture

TCFA=thin-cap fibroatheroma

UP=upstream

WSS=wall shear stress

Declarations

Acknowledgements: None.

Funding: None.

Conflicts of interest: H.O., J.S., A.K, T.T. and F.S. received honoraria for lectures. F.S. received a grant from Abbott Vascular. O.Y. and K.H. received grant support from Abbott Vascular. The other authors report no conflicts of interest.

Ethical approval: This study was conducted in agreement with the Declaration of Helsinki and was approved by the ethics committee of each institution.

Consent to participate: Not applicable

Consent for publication: Not applicable

Availability of data and material: Not applicable

Code availability: Not applicable

Authors' contributions: Not applicable

References

[1] Davies MJ, Thomas A (1984) Thrombosis and acute coronary-artery lesions in sudden cardiac ischemic death. N Engl J Med 310:1137-1140. https://doi.org/10.1056/NEJM198405033101801

[2] Kolodgie FD, Burke AP, Farb A, et al (2001) The thin-cap fibroatheroma: a type of vulnerable plaque: the major precursor lesion to acute coronary syndromes. Curr Opin Cardiol 16:285-292. https://doi.org/10.1097/00001573-200109000-00006

[3] Slager CJ, Wentzel JJ, Gijsen FJH, et al (2005) The role of shear stress in the generation of rupture-prone vulnerable plaques. Nat Clin Pract Cardiovasc Med;2:401-407. https://doi.org/10.1038/ncpcardio0274

[4] Kumar A, Thompson EW, Lefieux A, et al (2018) High coronary shear stress in patients with coronary artery disease predicts myocardial infarction. J Am Coll Cardiol 72:1926-1935.

[5] Fukumoto Y, Hiro T, Fujii T, et al (2008) Localized elevation of shear stress is related to coronary plaque rupture: a 3-dimensional intravascular ultrasound study with in-vivo color mapping of shear stress distribution. J Am Coll Cardiol 51:645-650.

[6] Jang IK, Bouma BE, Kang DH, et al (2002) Visualization of coronary atherosclerotic plaques in patients using optical coherence tomography: comparison with intravascular ultrasound. J Am Coll Cardiol 39:604-609.

[7] Richardson PD, Davies MJ, Born GV (1989) Influence of plaque configuration and stress distribution on fissuring of coronary atherosclerotic plaques. Lancet 2:941-944. https://doi.org/10.1016/S0140-

6736(89)90953-7

[8] Peiffer V, Sherwin SJ, Weinberg PD (2013) Does low and oscillatory wall shear stress correlate spatially with early atherosclerosis? A systematic review. Cardiovasc Res 99:242-250. https://doi.org/10.1093/cvr/cvt044

[9] Park JB, Choi G, Chun EJ, et al (2016) Computational fluid dynamic measures of wall shear stress are related to coronary lesion characteristics. Heart 102:1655-1661. http://dx.doi.org/10.1136/heartjnl-2016-309299

[10] Samady H, Eshtehardi P, McDaniel MC, et al (2011) Coronary artery wall shear stress is associated with progression and transformation of atherosclerotic plaque and arterial remodeling in patients with coronary artery disease. Circulation 124:779-788. https://doi.org/10.1161/CIRCULATIONAHA.111.021824

[11] Kolpakov V, Gordon D, Kulik TJ (1995) Nitric oxide-generating compounds inhibit total protein and collagen synthesis in cultured vascular smooth muscle cells. Circ Res 76:305-309. https://doi.org/10.1161/01.RES.76.2.305

[12] Death AK, Nakhla S, McGrath KCY, et al (2002) Nitroglycerin upregulates matrix metalloproteinase expression by human macrophages. J Am Coll Cardiol 39:1943-1950.

[13] Burke AP, Farb A, Malcom GT, Liang Y, Smialek JE, Virmani R (1999) Plaque rupture and sudden death related to exertion in men with coronary artery disease. JAMA 281:921-926. https://doi.org/10.1056/NEJM198405033101801

Figures

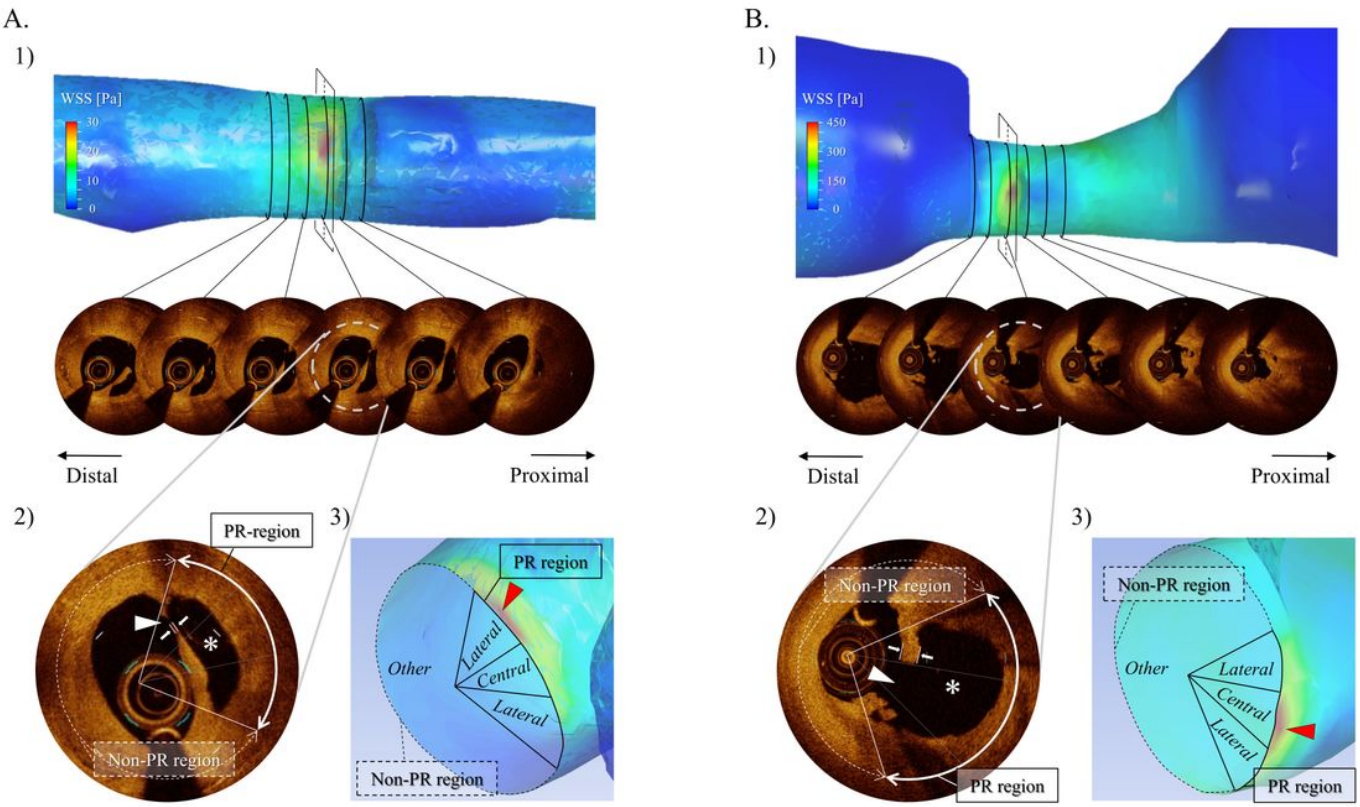

Figure 1

Representative cases of lateral-PR and central-PR (A) Representative case of lateral PR. Arrows indicate the thin remnant fibrous cap (30 μm). (B) Representative case of central PR. Arrows indicate the thick remnant fibrous cap (170 μm). The white arrowhead, asterisk, and red arrowhead indicate fibrous cap disruption, PR cavity, and location of peak WSS, respectively. CFD, computational fluid dynamics; OCT, optical coherence tomography; PR, plaque rupture; WSS, wall shear stress.

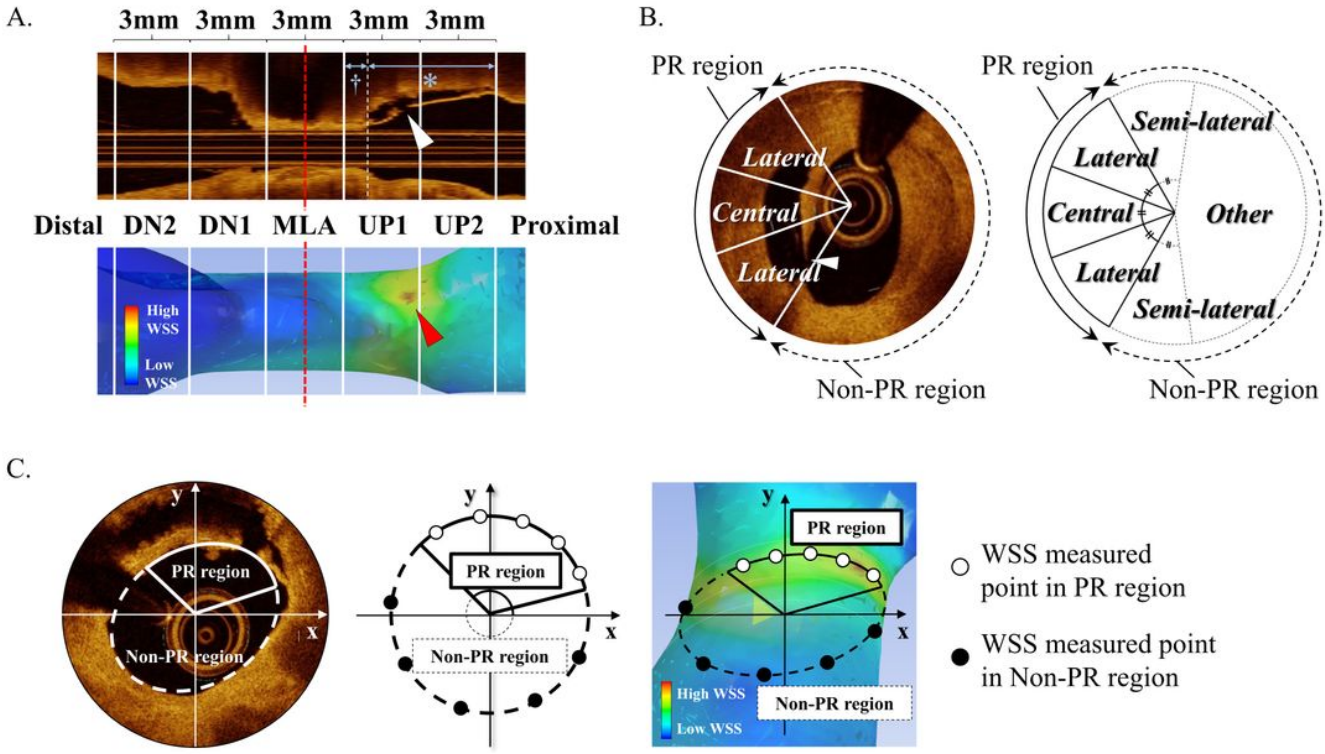

Figure 2

Relationships between WSS values and PR location (A) Longitudinal 3-mm segmental analysis. White arrowhead, PR site; red arrowhead, peak WSS site; asterisk, cross-sections with PR; dagger, cross-sections without PR. (B) Circumferential segmentation in peak WSS cross-section. (C) WSS measurement in PR and non-PR regions. DN, downstream; MLA, minimum lumen area; PR, plaque rupture; UP, upstream; WSS, wall shear stress.

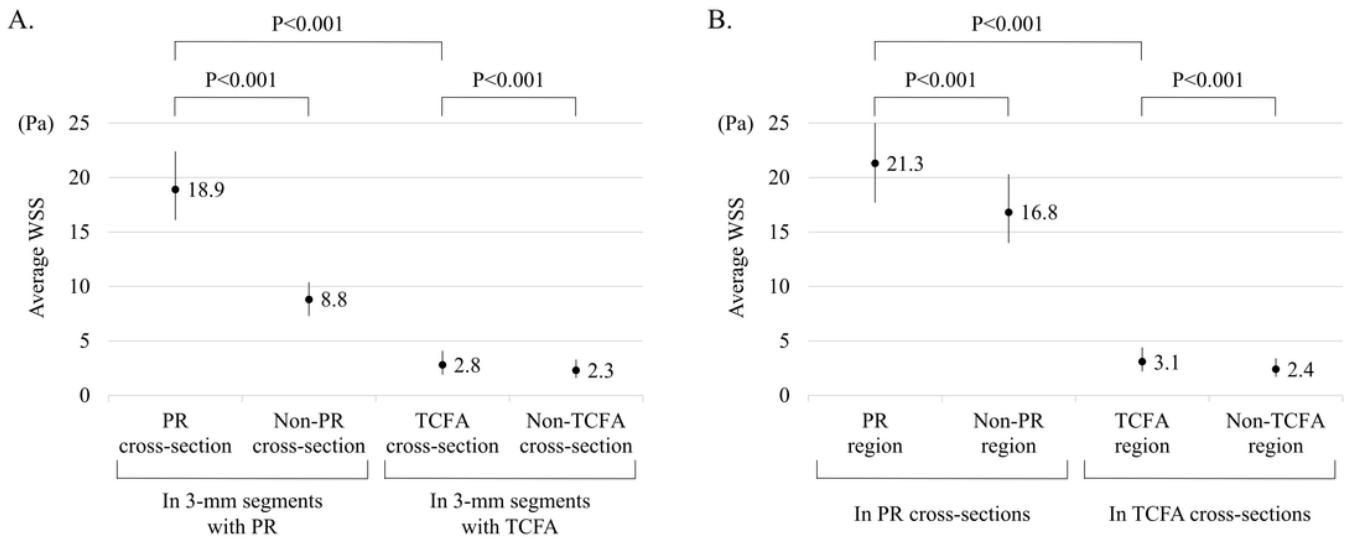

Figure 3

Relationship among WSS, PR, and TCFA (A) Comparisons of the average WSS in each cross-section: PR vs. non-PR, TCFA vs. non-TCFA, and PR vs. TCFA. (B) Comparisons of the WSS in each region: PR vs. non-PR, TCFA vs. non-TCFA, and PR vs. TCFA. PR, plaque rupture; TCFA, thin-cap fibroatheroma; WSS, wall shear stress.

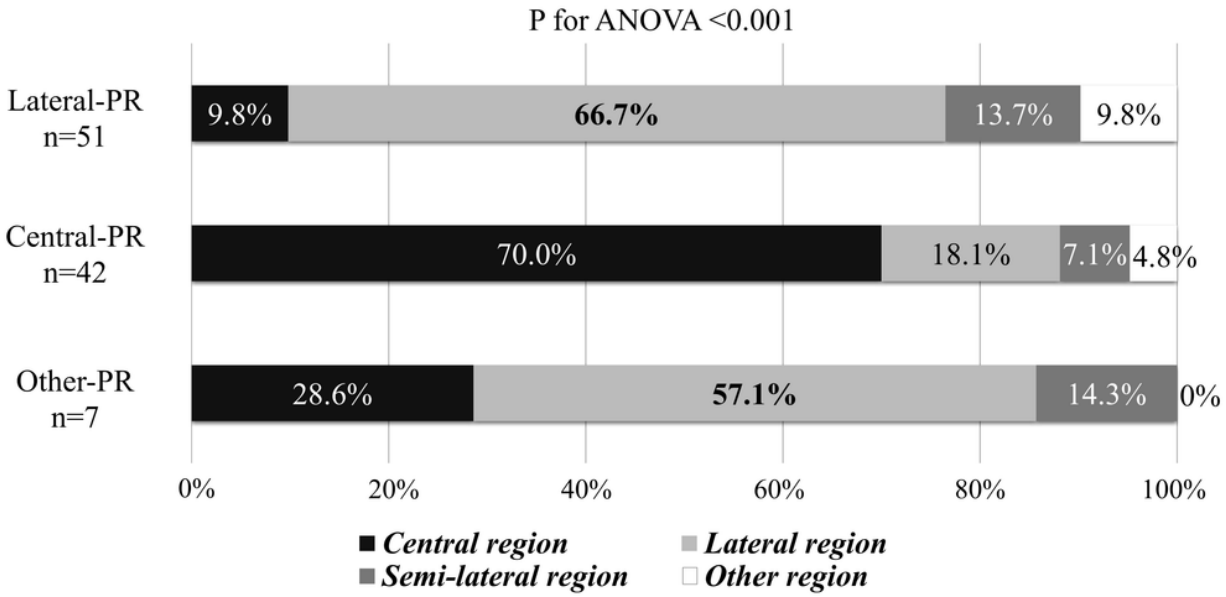

Figure 4

Relationship between the PR type and peak WSS location PR, plaque rupture; WSS, wall shear stress

Supplementary Files

This is a list of supplementary files associated with this preprint. Click to download.

- OnlineResource1.docx
- OnlineResource2.docx
- OnlineResource3.docx
- OnlineResource4.docx
- OnlineResource5.docx